Advanced Robotics, Vol. 20, No. 6, pp. 707–736 (2006)

Also available online - www.vsppub.com

Full paper

Experimental realization of dynamic walking of the biped humanoid robot KHR-2 using zero moment point feedback and inertial measurement

JUNG-YUP KIM *, ILL-WOO PARK and JUN-HO OH

HUBO Laboratory, Humanoid Robot Research Center, Department of Mechanical Engineering, Korea Advanced Institute of Science and Technology, 373-1 Guseong-dong Yuseong-gu, Daejeon 305-701, South Korea

Received 20 May 2005; accepted 1 September 2005

Abstract—This paper describes a novel control algorithm for dynamic walking of biped humanoid robots. For the test platform, we developed KHR-2 (KAIST Humanoid Robot-2) according to our design philosophy. KHR-2 has many sensory devices analogous to human sensory organs which are particularly useful for biped walking control. First, for the biped walking motion, the motion control architecture is built and then an appropriate standard walking pattern is designed for the humanoid robots by observing the human walking process. Second, we define walking stages by dividing the walking cycle according to the characteristics of motions. Third, as a walking control strategy, three kinds of control schemes are established. The first scheme is a walking pattern control that modifies the walking pattern periodically based on the sensory information during each walking cycle. The second scheme is a real-time balance control using the sensory feedback. The third scheme is a predicted motion control based on a fast decision from the previous experimental data. In each control scheme, we design online controllers that are capable of maintaining the walking stability with the control objective by using force/torque sensors and an inertial sensor. Finally, we plan the application schedule of online controllers during a walking cycle according to the walking stages, accomplish the walking control algorithm and prove its effectiveness through experiments with KHR-2.

Keywords: Dynamic walking; walking pattern; walking control; humanoid robot; KHR-2.

1. INTRODUCTION

Human walking is a repetitive process of ‘tilt over’ or unstable motions that could sometimes cause even a healthy man to fall down while walking on an uneven terrain. The walking process of humans was first studied as far back as the Second World War in the effort of developing artificial legs for disabled soldiers. Despite

*To whom correspondence should be addressed. E-mail: kirk1@mclab3.kaist.ac.kr

continuous research on the subject since then, we still do not clearly know how we walk stably. An important thing to mention here is that the biped walking mechanism is a complicated process to comprehend, and the high-level intellectual functions involved require infants to tirelessly practice for 1–2 years before they can stand and walk without losing stability.

Until recently, robots have often been seen in factories as manipulators for such tasks as welding, part-assembly, etc. These industrial robots have performed well-defined tasks within a framework based on economic efficiency and productivity. However, our desire of using robots has changed and continues to change with rapid industrial development. Today, it has become a norm that we expect robots to perform various tasks such as surgical operations, house cleaning, guidance, etc. We call robots with these capabilities human-friendly intelligent robots. Many kinds of intelligent robots have already been developed by many researchers since late 20th century. Among the many kinds of such robots, the humanoid-type robot is a representative human-friendly intelligent robot.

The two most important features of biped humanoid robots are the human-like shape and movements. Biped humanoid robots have two legs and are supposed to walk with a good mobile capability on various terrains including uneven surfaces or stairs. Thus, many researchers have developed humanoid robot platforms and have studied the biped walking of humanoid robots. The Honda humanoid [1–3], the WABIAN series of Waseda University [4, 5], H6,7 of Tokyo University [6, 7], HRP of AIST [8, 9] and JOHNNIE [10] are well-known human-scale biped humanoid robots. Mostly, the control strategy of dynamic walking of biped robots is based on the walking pattern generation, which considers the stable zero moment point (ZMP) trajectory and online balance control. As the actual ZMP trajectory is different from the desired ZMP trajectory due to reasons such as the unevenness of the surface, sensing errors and imperfect dynamic model of the robot, several online controllers based on the sensory feedback are required. Takanishi *et al.* studied online walking pattern generation and walking stabilized control by using upper body motion based on the ZMP information [4, 5]. Kajita *et al.* introduced a method of biped walking pattern generation by using a preview control of ZMP that uses future reference [8, 9]. Kagami *et al.* used a torso position compliance control method to track a given ZMP trajectory [6, 7]. In addition, many other research works on the stabilization control strategy of humanoid robots related to the angular momentum information have been published [12–14]. However, there have been relatively few research works on ZMP control and balance control using inertial measurement simultaneously.

In this paper, a dynamic walking control strategy is proposed for biped humanoid robots using the ZMP and inertial information. Our control scheme encompasses adaptive walking pattern generation, real-time ZMP compensation in the single support phase with damping control of the ankle joint, stable landing control and landing position control based on the angular velocity of the torso. In this manner,

a biped robot is able to adapt itself to uneven terrain without losing stability in real-time during walking.

This paper is organized as follows. In Section 2, we introduce the humanoid robot KHR-2 — its design concept, specifications and control system integration. Section 3 describes the standard walking pattern generation. Section 4 presents the dynamic walking algorithm and the online controllers. Finally, in Section 5, we show the experimental tests to verify the effectiveness of the proposed controllers and the overall dynamic walking control strategy.

2. OVERVIEW OF KHR-2 (KAIST HUMANOID ROBOT-2)

2.1. Mechanical design

KHR-2 was developed according to the following design philosophy (Fig. 1):

(i) Human-like shape and movements.
(ii) Lightweight, compact size and backlash-free actuators.
(iii) Self-contained system.
(iv) Kinematically simple structure.
(v) Low power consumption.

KHR-2 is supposed to be a human-friendly intelligent robot. Thus, we made it resemble a child-sized human, which has enough joints to imitate human motions. The decision for the child-size came from the concerns of practicality, power

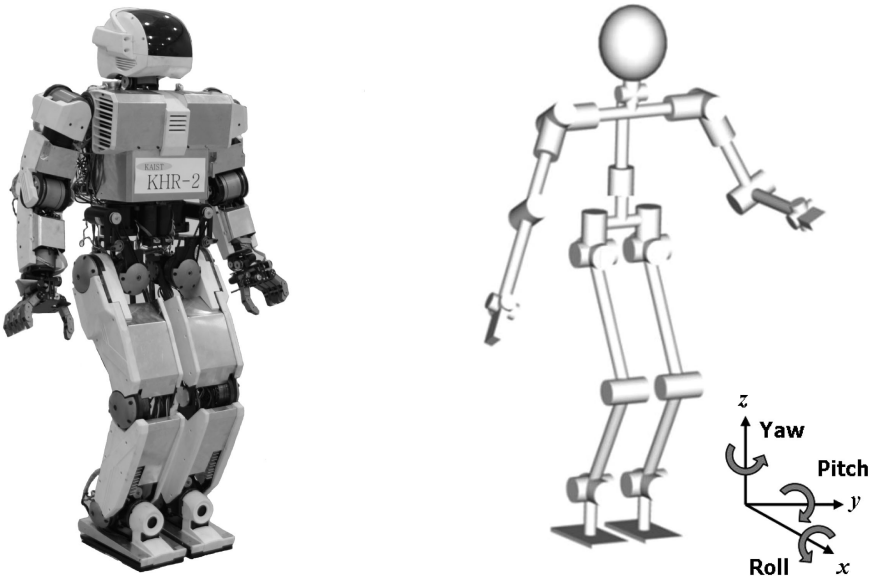

Figure 1. Photograph of the biped humanoid robot KHR-2 and its joint structure (with the orientation).

Table 1.
Degrees of freedom and dimensions of KHR-2

Head	eye (pan and tilt)	2 d.o.f. × 2 = 4 d.o.f.
	neck (pan and tilt)	2 d.o.f.
Arm	shoulder (roll/pitch/yaw)	3 d.o.f. ×2 = 6 d.o.f.
	elbow (pitch)	1 d.o.f. × 2 = 2 d.o.f.
Hand	wrist (roll/pitch)	2 d.o.f. ×2 = 4 d.o.f.
	finger	1 d.o.f. × 5 × 2 = 10 d.o.f.
Torso	waist (yaw)	1 d.o.f.
Leg	hip (roll/pitch/yaw)	3 d.o.f. × 2 = 6 d.o.f.
	knee (pitch)	1 d.o.f. × 2 = 2 d.o.f.
	ankle (roll/pitch)	2 d.o.f. × 2 = 4 d.o.f.
Total		41 d.o.f.
Dimensions	height	1200 mm
	width (shoulder to shoulder)	420 mm
	depth (chest to back)	213 mm
	length of upper arm	184 mm
	length of lower arm	185.5 mm
	length of upper leg	290 mm
	length of lower leg	280 mm

efficiency and human-friendliness. The weight, height and total degrees of freedom of KHR-2 are 56 kg, 120 cm and 41 d.o.f. KHR-2 is actuated by DC motors through harmonic drive reduction gears that provide compactness and better controllability with reduced backlash. The main controller, motor controllers, sensory devices, battery, etc., are all built in to KHR-2 to make it a self-contained robot. For the simple closed-form solution of inverse kinematics, all joint axes are made to cross each other at one point. Finally, the size and thickness of the frame structure were minimized within sufficient stiffness and all controllers were designed under consideration to electrical efficiency. The degrees of freedom and dimensions of the robot are summarized in Table 1.

2.2. Control system integration

A distributed control system was built for KHR-2 because it has many joints, sensors and peripheral devices, such as a vision system, wireless LAN (local area network), CAN (controller area network) interface card, speaker, microphone, etc. By using distributed control architecture, the computational burden on the main controller was decreased effectively at the expense of having to develop subcontrollers and communication bus lines between the main controller and subcontrollers. We used a commercial single-board computer as the main controller, which has fast computing speed (933 MHz), compact size (3.5 in^2), low power consumption (19 W), various peripheral interfaces, and an easy and fast programming environment in Windows XP. Note that since Windows XP is a general purpose operating system, its timer is not deterministic and has a low priority. Hence, to guarantee real-time

capability in Windows XP, we used a RTX (Real Time eXtension; Venturcom Co.) program which is a HAL (Hardware Abstraction Layer) extension commercial software. This software allows us to make the timer interrupt service routine with the highest priority so that the user can control the robot in real-time. For the communication bus line, a CAN protocol was established between the main computer and the subcontrollers, such as the motor controllers and sensory devices. These motor controllers and the sensory devices of KHR-2 are summarized in Table 2. Consequently, KHR-2 is tele-operated by a laptop computer with a wireless LAN. Figure 2 shows the overall system configuration of KHR-2.

Table 2.
Motor controllers and sensors of KHR-2

	Description
Two-channel motor controller	high-power motor controller (400 W/channel) for legs, arms and torso
Seven-channel motor controller	low-power motor controller (48 W/channel) for head and hands
Force/Torque sensor	measurement of ZMP and external loads of the hands
Inertial sensor	measurement of angular position and velocity of torso
Tilt sensor	measurement of the ground inclination and acceleration of foot
CCD camera	image processing (object recognition and visual servoing)

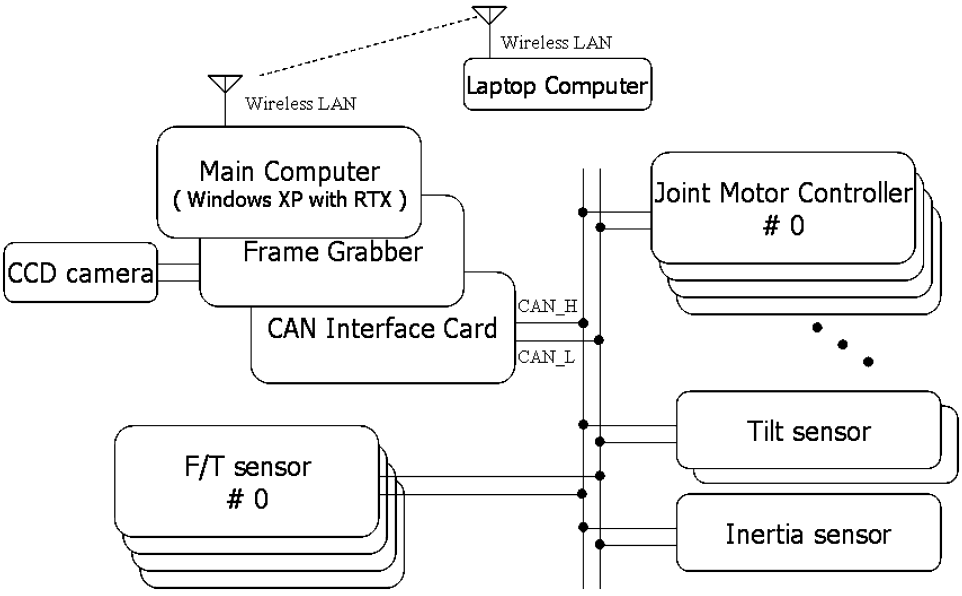

Figure 2. Overall system configuration of KHR-2.

3. WALKING PATTERN GENERATION

3.1. Motion control process

The position of each motor is PD controlled by using encoder feedback. To control all 41 motors smoothly, it is important that the main computer sends the reference positions at exact time intervals. In KHR-2, the main computer sends the reference position data to all motor controllers simultaneously at an interval of 10 ms (100 Hz). Then, each motor controller interpolates linearly the reference position data at an interval of 1 ms (1 kHz). Conversely, the sensory devices send their information back to the main computer at a frequency of 100 Hz. Figure 3 shows the outline of the motion control process.

3.2. Walking-ready pose

A walking-ready pose is a basic pose of KHR-2 before walking. For the walking-ready pose, KHR-2 lowers his pelvis by bending the knee joints of the legs. The reason is to prevent the singularity problem of inverse kinematics and realize stable walking with a constant height of the pelvis by considering the gait geometry. Note that the height of the pelvis is related to the dynamic characteristics of the robot. When the robot is walking, it is periodically in the single-support phase. In the single-support phase, the robot can be assumed as a simple inverted pendulum model on the coronal plane and its natural frequency is written as:

$$f = \frac{1}{2\pi}\sqrt{\frac{g}{l}}\ (\text{Hz}), \tag{1}$$

where g and l are the acceleration due to gravity and the height of the center of mass of the robot from the ground, respectively. Of course, the natural frequency of a simple inverted pendulum exists theoretically because the mass will fall down. However, this inverted pendulum model does not fall down during biped walking and is periodically tilted sideward. Therefore, we determined the walking period according to (1) for smooth biped motion and efficient energy consumption. In this

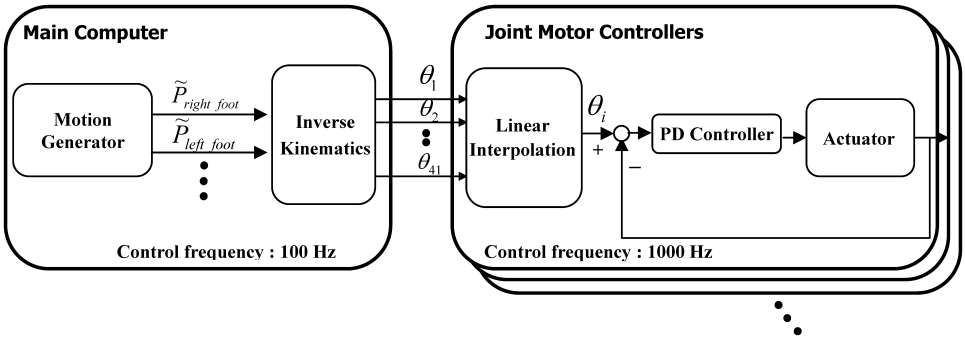

Figure 3. The motion control process of KHR-2.

research, the lowering value is 40 mm, so l is about 0.9 m and then the natural frequency is 0.526 Hz.

3.3. Essential factors of the walking pattern

Three basic factors for the design of the standard walking pattern are defined as follows:

(i) Walking period (stride time, stride time = step time × 2).

(ii) Double-support ratio: portion of double-support phase in a walking cycle (Fig. 4).

(iii) Lateral swing amplitude of the pelvis.

We set the walking period of KHR-2 to 1.9 s because its natural frequency is 0.526 Hz. The portion of the double-support phase in a walking cycle is about 10–20% for humans [11], whereas for KHR-2 we experimentally determined its value to be 5% because KHR-2 does not have any toe joints. The lateral swing motion of the pelvis is essential to move the ZMP to each sole during walking. In the case of an adult, the human walking cycle at 60 steps/min causes the pelvis to swing at an amplitude of about 6 cm. The interesting thing here is that the swinging amplitude of the pelvis tends to decrease as the walking speed increases [11]. This reason will be explained later. Consequently, the lateral swing amplitude of the pelvis for KHR-2 is set to 6.4 cm with a step frequency of 63 steps/min (0.95 s/step).

3.4. Standard walking pattern

First of all, we established the coordinates system of KHR-2 (Fig. 5). The body-fixed coordinate system is attached in the pelvis center, so it is used to indicate the relative positions of the two feet from the pelvis. A ground-fixed coordinate indicates the absolute positions of the pelvis and the two feet from a specific point on the ground.

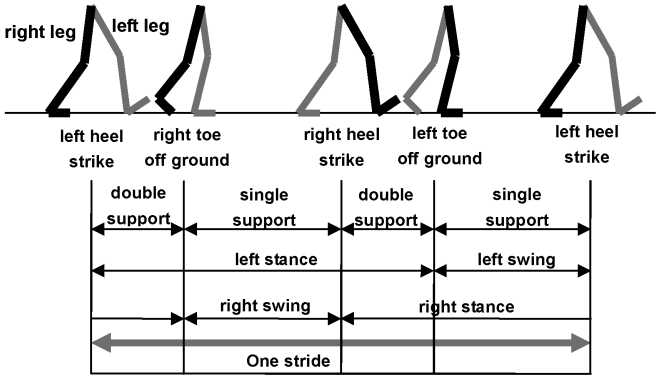

Figure 4. Walking cycle (stride) [16].

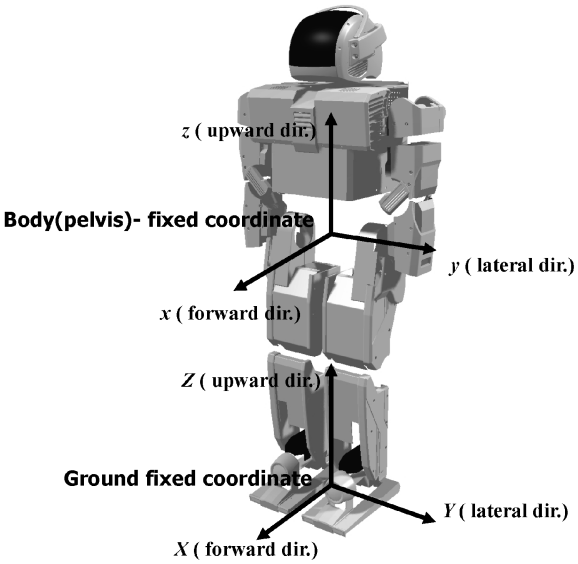

Figure 5. The coordinates system of KHR-2.

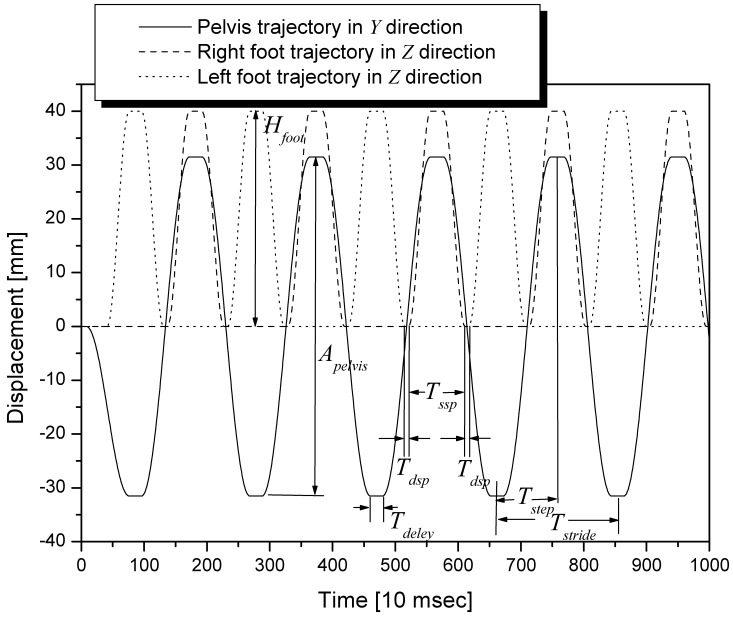

(a)

Figure 6. Standard forward walking pattern with a stride of 40 cm and a step time of 0.95 s. (a) Upward and lateral trajectories of the feet and the pelvis. (b) Absolute trajectories of the feet. (c) Relative trajectories of the feet.

In accordance with the three factors, we designed the trajectories for the pelvis and two feet (Fig. 6). For the pelvis, the lateral (Y-direction) path of the ground-fixed coordinate was generated by using the cosine function in order to produce a smooth curve and to eliminate velocity discontinuity. For the two feet, each foot needs upward (Z-direction) trajectories of the ground-fixed coordinate. The maximum elevation of the foot is 40 mm and its upward trajectory is also generated by using

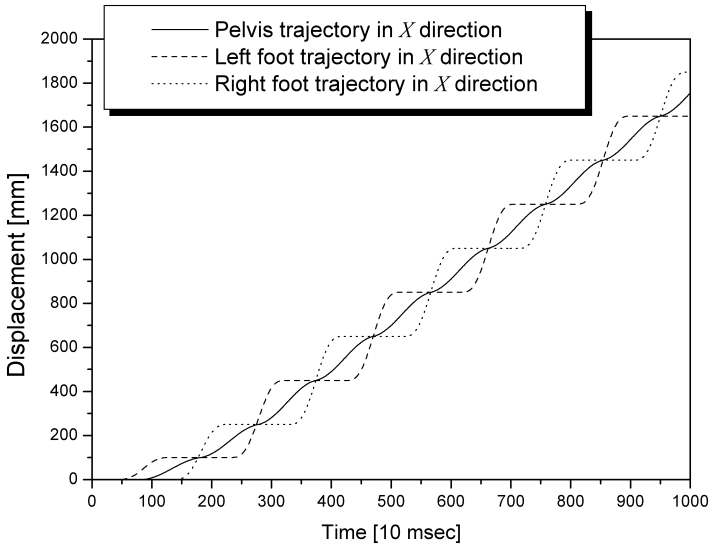

(b)

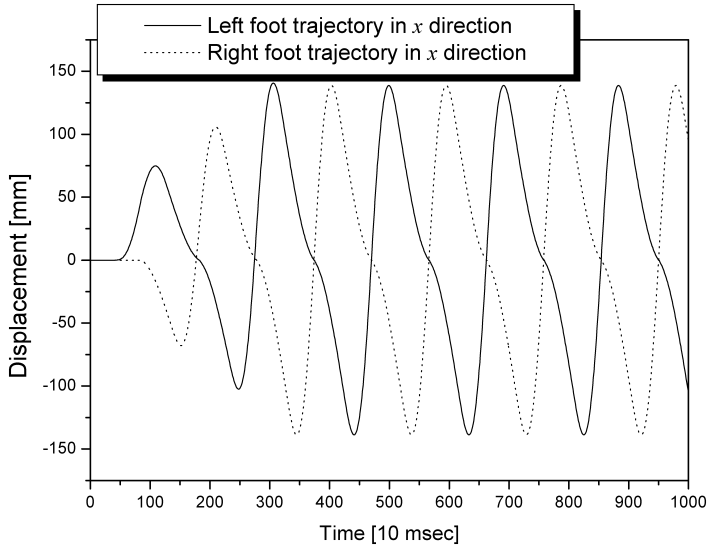

(c)

Figure 6. (Continued).

Table 3.
Dimensions of the standard walking pattern of forward walking

	Description	Value
A_{pelvis}	lateral swing amplitude of pelvis	64 (mm)
H_{foot}	maximum elevation of foot	40 (mm)
T_{stride}	walking period (stride time)	1.9 (s)
T_{step}	step time	0.95 (s)
T_{delay}	delay time	0.1 (s)
κ_{dsp}	double-support ratio	0.05 (5%)
T_{ssp}	single-support time	$T_{\text{step}} \times (1.0 - \kappa_{\text{dsp}})$
T_{dsp}	double-support time	$T_{\text{step}} \times \kappa_{\text{dsp}}$

the cosine function. The dimensions of the standard walking pattern of forward walking are given in Table 3. It is important to note that repetitive short periods of delay time T_{delay} exist around the maximum and minimum lateral displacements of the pelvis. T_{delay} lengthens the static period of walking motion by reducing the dynamic period for better walking stability.

Next, the forward walking pattern is completely designed by adding forward (x-direction) trajectories of two feet in the body-fixed coordinate. Note it is somewhat confusing to think of the walking path of the robot from the positions of the feet in the body-fixed coordinate. Hence, we designed the forward (X-direction) trajectories of the two feet and pelvis in the ground-fixed coordinate first, and then converted them into the forward trajectories of the two feet in the body-fixed coordinate. As for absolute trajectories of the two feet in the forward direction, we used a cycloid function. Figure 7a shows the foot trajectory with a step length of 200 mm during one step time. As for the absolute trajectory of the pelvis in the forward direction, it is generated by mixing the cosine and linear function with an appropriate ratio. Figure 7b shows the pelvis trajectory with a step length of 200 mm during one step time. The reason why we have used a cycloid function for the foot trajectory is that the cycloid function describes a path of a certain point on the circumference of a circle during circling, considering that the human ankle is circling the tiptoe. Finally, relative trajectories of the two feet are derived following the relationships:

$$\text{relative foot path} = \text{absolute foot path} - \text{absolute pelvis path}. \tag{2}$$

4. DYNAMIC WALKING CONTROL

4.1. Walking stages

We defined the following five walking stages that are required to control the humanoid efficiently in various situations. In each stage, we can easily recognize the current movement and then predict the next movement. Stages 1–4 are repeated

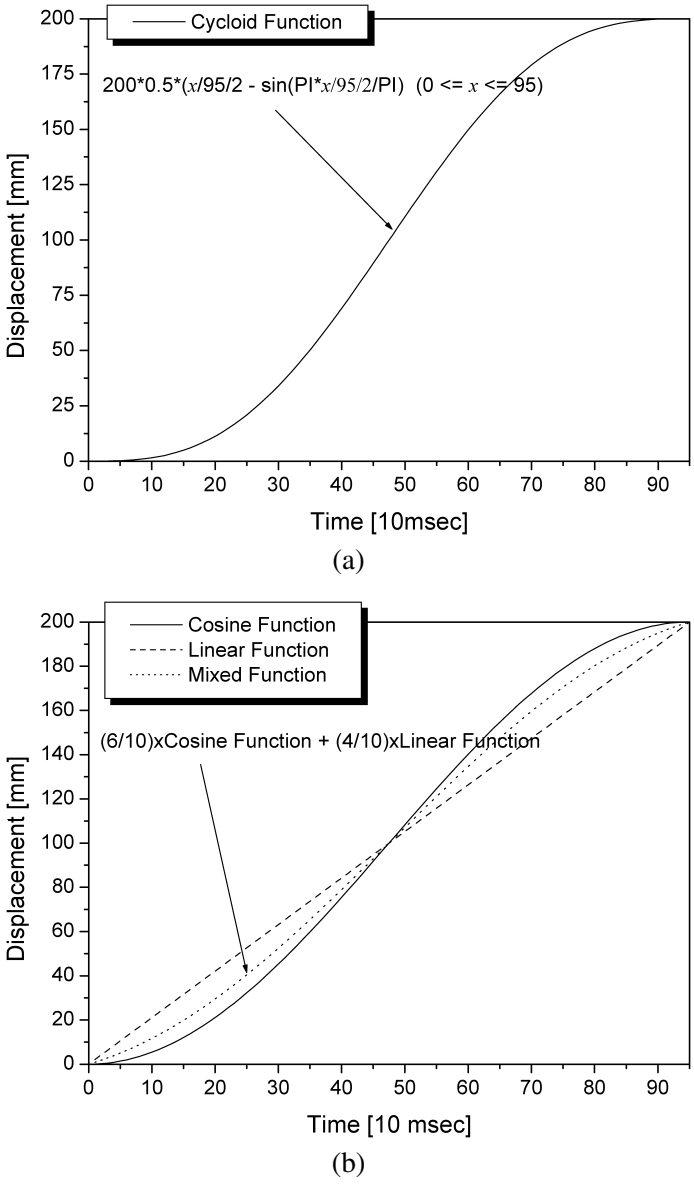

Figure 7. Absolute trajectories of (a) the foot and (b) the pelvis in the X-direction during one step time (stride: 40 cm).

during walking. Stage 5 is the period of standstill pose. These stages are described below referring to Fig. 8:

- Stage 1: lift the left leg to its maximum flexion and height.
- Stage 2: lower the left leg until it makes complete contact with the ground.
- Stage 3: lift the right leg to its maximum flexion and height.

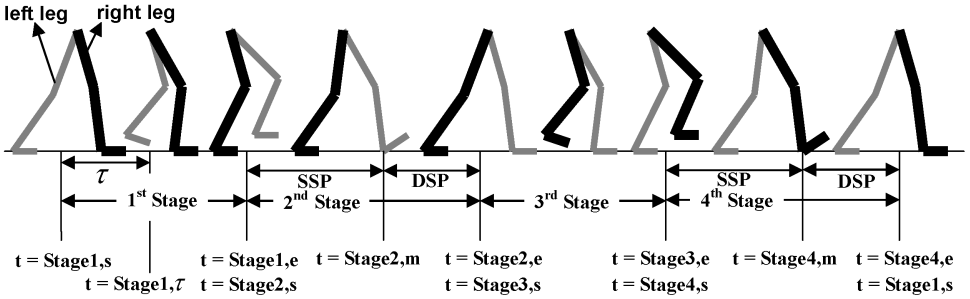

Figure 8. Walking stages and time table.

Table 4.
The time schedule of online controllers

Control scheme	Online controller	Stage 1	Stage 2		Stage 3	Stage 4	
			SSP	DSP		SSP	DSP
Real-time	damping controller	√	√		√	√	
balance control	ZMP compensator	√	√		√	√	
	soft landing controllers			√			√
Walking pattern	pelvis swing amplitude controller			√			√
control	torso pitch/roll controller			√			√
Predicted	tilt over controller	√			√		
motion control	landing position controller		√	√		√	√

SSP and DSP stand for the single-support phase and the double-support phase, respectively.

- Stage 4: lower the right leg until it makes complete contact with the ground.
- Stage 5: Follows after Stage 1 or 3 and brings the robot to the stop pose with both legs landed on the ground.

In these stages, we grasped the features of dynamic motion and then developed the appropriate controllers for stable walking. Table 4 shows the time schedule of the online controllers.

4.2. Real-time balance control

4.2.1. Damping controller. The real-time balance control scheme consists of four kinds of online controllers. First, the damping controller is designed to eliminate the sustained oscillation in the single-support phase [17]. This oscillation is mainly caused by the force/torque sensor which is installed at the ankle joints as part of the compliant motion structure. In addition, the leg is flexible and relatively long compared with the cross-section of the humanoid. Hence, we modeled the robot as a simple inverted pendulum with a compliant joint and designed a damping controller to impose the damping forces at the ankle joints without any change of the steady-state value of the joint angle. Figures 9 and 10 show the mathematical modeling and the control block diagram, respectively. In Fig. 9, l is the distance

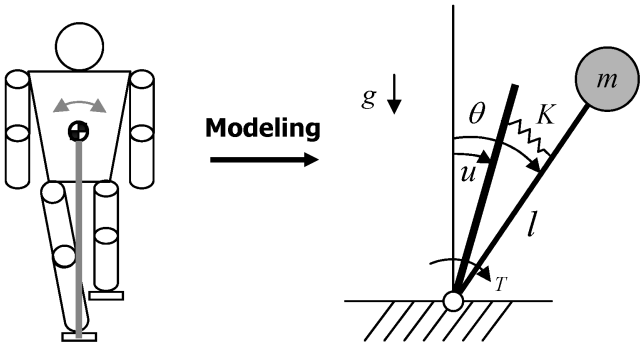

Figure 9. Simple inverted pendulum model with a compliant joint in the single-support phase [17].

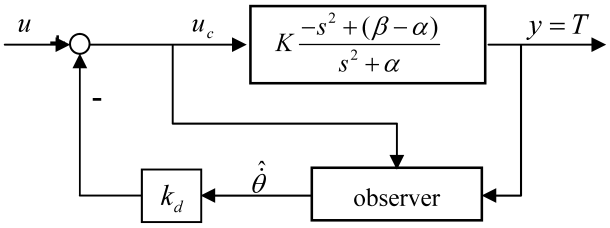

Figure 10. Block diagram of the damping control.

from the ground to the center of mass, m is the equivalent mass, u is the reference joint angle, θ is the actual joint angle due to the compliance, K is the stiffness of the leg, T is the measured torque and g is the acceleration due to gravity. In Fig. 10, α is $K/ml^2 - g/l$, β is K/ml^2, k_d is a damping control gain and u_c is a compensated joint angle. The equation of motion and the damping control law can be written as:

$$T = mgl\theta - ml^2\ddot{\theta} = K(\theta - u), \tag{3}$$

$$u_\mathrm{c} = u - k_\mathrm{d}\hat{\dot{\theta}}. \tag{4}$$

4.2.2. ZMP compensator. We designed the ZMP compensator in the single-support phase because the damping controller alone would not be sufficient to maintain stable walking due to the inevitable movement of the ZMP. If the ZMP is stabilized by the ZMP compensator according to the ZMP dynamics (5) of the simple inverted pendulum with a compliant joint, the torso will move back and forth and from side to side. However, if we eliminate the oscillation of the torso by using the damping controller, the ZMP will move back and forth and from side to side. In (5), Y_pelvis is the lateral displacement of the pelvis, l is the distance from the ground to the center of mass, g is the acceleration due to gravity and Y_ZMP is the lateral ZMP. Consequently, we have to control both torso movement and ZMP

simultaneously:

$$Y_{\mathrm{ZMP}} = Y_{\mathrm{pelvis}} - \frac{l}{g}\ddot{Y}_{\mathrm{pelvis}}. \tag{5}$$

To compensate for the ZMP error, the pelvis displacement is used as the control input (Fig. 11). That is, we compensate the X-component and Y-component of the ZMP by moving the pelvis in the forward and lateral directions on the transverse plane. First, transfer functions are derived by experimental frequency response analysis in the presence of the damping control. From Figs 12 and 13 of the experimental results, the magnitudes have peak values at a frequency of 10 rad/s and a phase of $-180°$. The phase angles converge to $-360°$ at high frequency. Therefore, it became clear that these transfer functions are fourth-order and type 0 systems, and each system can be assumed to have double inverted pendulum dynamics. We mathematically modeled each system as a fourth-order system which

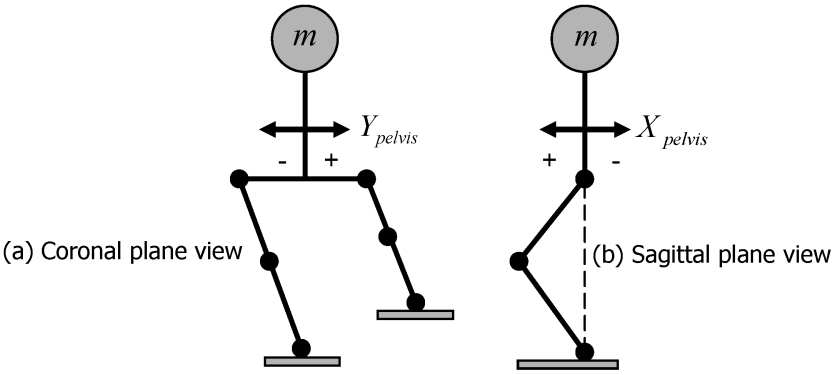

Figure 11. Double inverted pendulum model in the single-support phase.

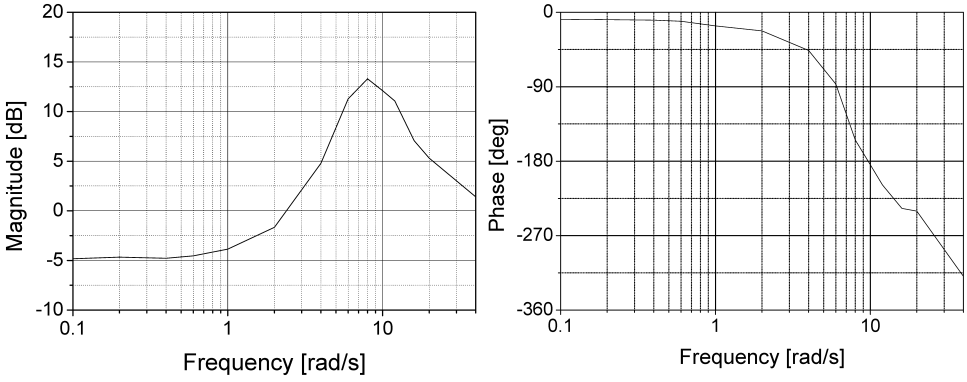

Figure 12. Bode plot of the transfer function ($X_{\mathrm{ZMP}}/X_{\mathrm{pelvis}}$) in the single-support phase.

has two double poles as follows:

$$\frac{Y_{\text{ZMP}}}{Y_{\text{pelvis}}} = G_Y(s) = \frac{28541.65}{(s^2 + 4.59s + 131.52)^2}, \tag{6}$$

$$\frac{X_{\text{ZMP}}}{X_{\text{pelvis}}} = G_X(s) = \frac{6668.34}{(s^2 + 3.68s + 106.77)^2}. \tag{7}$$

Next, ZMP compensators in the single-support phase are designed by using the pole placement technique. To realize the arbitrary pole assignment, we determined to design fifth-order compensators. Figure 14 shows the feedback control block diagram in that ZMP_{ref} is the reference ZMP, $C(\text{s})$ is the compensator and $G(\text{s})$ is the transfer function. u_{pelvis} and u_{comp} are the prescribed displacement and the compensatory displacement of the pelvis on transverse plane, respectively. Consequently, pelvis displacements from the standard walking pattern and compensator are superimposed in real-time. Each compensator has a integrator, $1/(s + a)$ (a is a non-zero positive integer), which helps to prevent steady-state error and improve continuity of the compensatory input. The compensators are designed as follows:

X_{ZMP} compensator:

$$C_X(s) = \frac{-62.065\text{s}^4 - 3020.8s^3 - 35673.5s^2 - 355565.5s - 1196033.3}{s^5 + 70.44s^4 + 2255.6s^3 + 40240.4s^2 + 376617.8s + 1118129.2}. \tag{8}$$

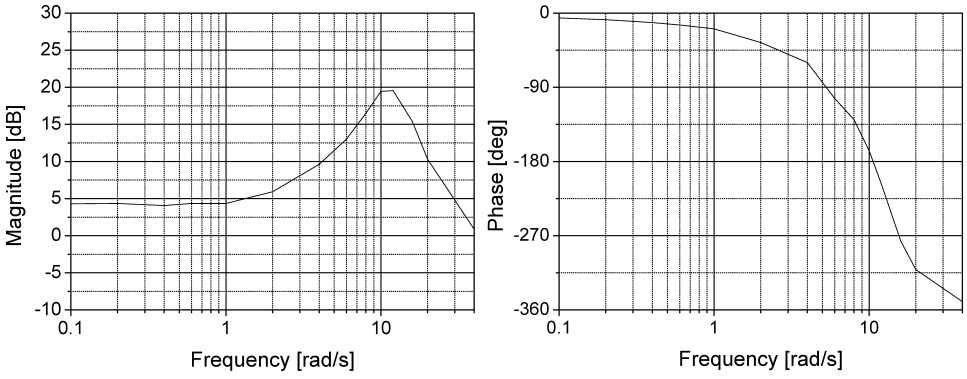

Figure 13. Bode plot of the transfer function ($Y_{\text{ZMP}}/Y_{\text{pelvis}}$) in the single-support phase.

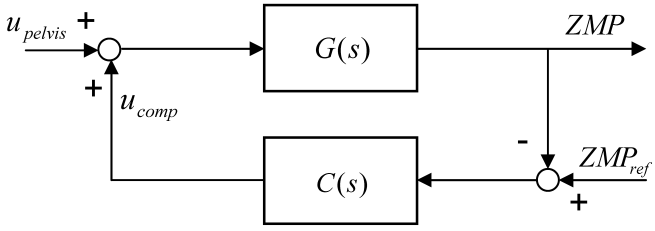

Figure 14. ZMP compensation diagram.

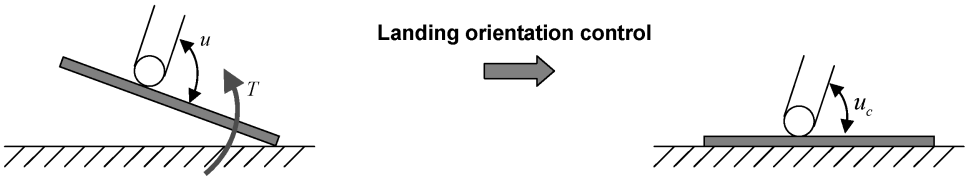

Figure 15. Landing orientation control.

Y_{ZMP} compensator:

$$C_Y(s) = \frac{-34.97\mathrm{s}^4 - 1396s^3 - 18287.5s^2 - 185137.6s - 607515.1}{s^5 + 80s^4 + 2831.7s^3 + 54573.2s^2 + 530148.6s + 1593487.3}. \quad (9)$$

4.2.3. Landing orientation controller. We applied soft landing control, which consists of landing orientation control and landing timing control [17]. The landing orientation controller integrates the measured torque over time to achieve soft landing and stable contact by adapting the ankle joints to the ground surfaces (Fig. 15). The control law of the landing orientation control is:

$$u_{\mathrm{c}} = u + \frac{T(s)}{C_{\mathrm{L}}s + K_{\mathrm{L}}}, \quad (10)$$

where T is the measured torque, C_{L} is the damping coefficient, K_{L} is the stiffness, u is the reference angle of ankle and u_{c} is the compensated reference angle of ankle.

4.2.4. Landing timing controller. The landing timing controller prevents the robot from being unstable during landing by modification of the walking pattern schedule. That is, if the foot does not land on the ground at the end of Stage 2 and 4 as the prescribed schedule, the time scheduler of the main computer will pause the motion flow until the foot contacts the ground. Therefore, the real walking motion can follow the prescribed walking pattern despite anomalies emerging during walking.

4.3. Walking pattern control

4.3.1. Pelvis swing amplitude controller. The walking pattern control scheme comprises two kinds of online controllers — the pelvis swing amplitude controller and the torso pitch/roll controller. In the human walking pattern, the pelvis swing amplitude becomes small with fast walking. This is because the lateral inertial force of the human becomes large when the lateral acceleration is increased due to high walking speed. That is, in (5), if the lateral acceleration rises or the center of mass is high, a little lateral displacement of the pelvis is sufficient to shift the ZMP to each sole. From this point of view, we periodically adjust the lateral pelvis swing amplitude to move the ZMP properly by measuring the ZMP during each walking cycle. The principle is describes as follows referring to Fig. 16:

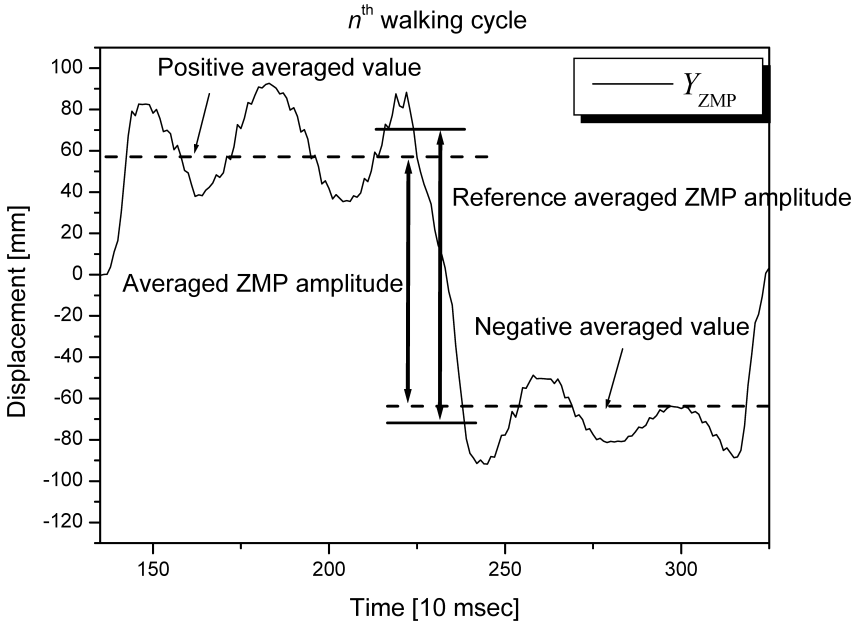

Figure 16. Pelvis swing amplitude control.

(i) Calculate the average values of the positive and negative ZMP during the nth walking cycle.

(ii) Derive the nth averaged ZMP amplitude.

(iii) Modify the lateral pelvis swing amplitude in the $(n + 1)$th walking cycle by adding the compensatory amplitude using a PI controller.

In this manner, the averaged ZMP amplitude can be converged to the reference averaged ZMP amplitude. The control law is written as follows:

$$A_{\mathrm{c}}^{\mathrm{pelvis}}(n+1) = A_{\mathrm{pelvis}} + ZMP_{\mathrm{err}}(n) \cdot \left(k_{\mathrm{p}} + \frac{k_{\mathrm{I}}}{s}\right), \tag{11}$$

$$ZMP_{\mathrm{err}} = Y_{\mathrm{ref\ ZMP}} - \frac{1}{T_{\mathrm{step}}} \left(\int_{\mathrm{Stage3,s}}^{\mathrm{Stage4,e}} Y_{\mathrm{ZMP}}\, \mathrm{d}t - \int_{\mathrm{Stage1,s}}^{\mathrm{Stage2,e}} Y_{\mathrm{ZMP}}\, \mathrm{d}t \right), \tag{12}$$

where A_{pelvis} is the standard lateral pelvis swing amplitude, $A_{\mathrm{c}}^{\mathrm{pelvis}}(n+1)$ is the compensated lateral pelvis swing amplitude in the $(n + 1)$th walking cycle, $Y_{\mathrm{ref\ ZMP}}$ is the reference averaged ZMP amplitude, Y_{ZMP} is the y-component of the ZMP, T_{step} is the step time, and k_{p} and k_{I} are proportional and integral gains, respectively.

4.3.2. Torso roll/pitch controller. When a biped humanoid robot is walking, swaying motions of the torso in the lateral and forward directions will occur. This

motion can be inclined toward the positive side or negative side if the dynamic walking is not adequately balanced against the slope of the ground. Then, it is necessary to adjust the walking pattern. Accordingly, it is necessary for the center position of the pelvis to move to the opposite direction from the inclined side on the transverse plane so that the torso swaying movement can be balanced well on inclined surfaces. In this controller, the inertial sensor is used to measure the torso movement during every walking cycle. The principle is as follows:

(i) Integrate over time the angular position value of the torso in each single-support phase (Stage1, s–Stage2, m or Stage3, s–Stage4, m) during the nth walking cycle referring to Fig. 8.

(ii) Calculate the forward and lateral differences between the right foot swing phase and the left foot swing phase during the nth walking cycle.

(iii) Modify the pelvis center position in the $(n + 1)$th walking cycle by integral control of differences.

In this manner, the pelvis center position is adjusted gradually according to the inclination of the ground. The control law is written as follows:

$$\tilde{P}^{\text{pelvis}}(n+1) = \tilde{\theta}^{\text{torso}}_{\text{err}}(n) \cdot \frac{K_{\text{I}}}{s}, \tag{13}$$

$$\tilde{P}^{\text{pelvis}} = \begin{pmatrix} P_X^{\text{pelvis}} \\ P_Y^{\text{pelvis}} \end{pmatrix}, \quad \tilde{\theta}^{\text{torso}}_{\text{err}} = \begin{pmatrix} -\left(\int_{\text{Stage1,s}}^{\text{Stage2,m}} \theta_{\text{p}}^{\text{torso}} \, \mathrm{d}t + \int_{\text{Stage3,s}}^{\text{Stage4,m}} \theta_{\text{p}}^{\text{torso}} \, \mathrm{d}t \right) \\ -\left(\int_{\text{Stage1,s}}^{\text{Stage2,m}} \theta_{\text{r}}^{\text{torso}} \, \mathrm{d}t + \int_{\text{Stage3,s}}^{\text{Stage4,m}} \theta_{\text{r}}^{\text{torso}} \, \mathrm{d}t \right) \end{pmatrix}$$

$$\text{and} \quad K_{\text{I}} = \begin{pmatrix} k_{\text{I,p}} \\ k_{\text{I,r}} \end{pmatrix},$$

where $\tilde{P}^{\text{pelvis}}$ is the center position vector of the pelvis on the transverse plane in the ground-fixed coordinate, $\theta_{\text{p}}^{\text{torso}}$ and $\theta_{\text{r}}^{\text{torso}}$ are the torso pitch and roll angles (Fig. 17) and K_{I} is the integral gain matrix.

4.4. Predicted motion control

4.4.1. Landing position controller. The predicted motion control is based on the expected movements of the robot and it is needed to prevent abnormal movements. Another feature of this control scheme is that its synthesis demands a lot of experimental results. This means that we anticipate future movements by means of the experimentally statistical information and then try to prevent the abnormal conditions by exercising additional motions. There are two online controllers in this control method — the landing position controller and the tilt over controller. All these controllers are based on the inertial sensor. The landing position controller is

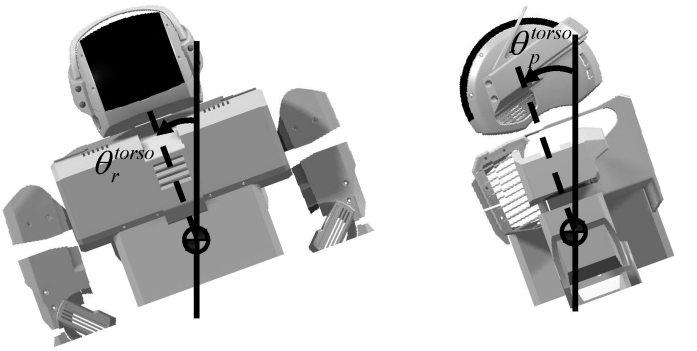

Figure 17. Roll and pitch angles of the torso.

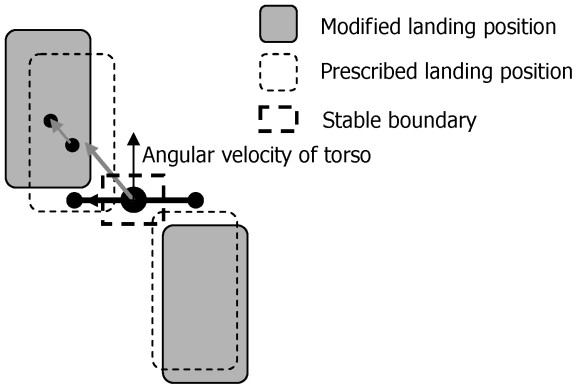

Figure 18. Landing position control.

used to compensate for the contact position on the ground by measuring the angular velocity. A fundamental mechanism of human walking is that the foot moves toward the falling direction to prevent falling down. This falling direction is not the same in each step during forward walking. In other words, it is not deterministic. For example, it is easily observable that we do not step on the same position on the ground during marking time. This is because humans adjust the step position by use of the vestibular organs. Analogously, in KHR-2, the landing position controller compensates for the foot landing position on the ground in order to step toward the falling direction (Fig. 18). The falling direction is determined by averaging the angular velocity of the torso for a little time from the time of stage2,s or stage4,s referring to Fig. 8. During the expected remaining time up to the contact, the robot moves the foot to a new position if the average velocity exceeds the stable bound which was already specified from experimental results. The schematic of the landing position controller is shown in Fig. 18. The control law is defined as

follows:

$$\tilde{P}_m^{\text{foot}}(n) = \tilde{P}^{\text{foot}}(n) + k_{\text{p}}\tilde{\dot{\theta}}_{\text{err}}^{\text{torso}}, \tag{14}$$

$$\tilde{P}^{\text{foot}} = \begin{pmatrix} P_x^{\text{foot}} \\ P_y^{\text{foot}} \end{pmatrix}, \ \tilde{\dot{\theta}}_{\text{err}}^{\text{torso}} = \begin{pmatrix} \dot{\theta}_{\text{p,avg}}^{\text{torso}} - \dot{\theta}_{\text{p,stable}}^{\text{torso}} \\ \dot{\theta}_{\text{r,avg}}^{\text{torso}} - \dot{\theta}_{\text{r,stable}}^{\text{torso}} \end{pmatrix},$$

where $\tilde{P}^{\text{foot}}(n)$ and $\tilde{P}_m^{\text{foot}}$ are the prescribed and modified landing position vector of the n-th foot step in the body-fixed coordinate, $\dot{\theta}_{\text{p,avg}}^{\text{torso}}$ and $\dot{\theta}_{\text{r,avg}}^{\text{torso}}$ are the averaged pitching and rolling angular velocity of the torso, $\dot{\theta}_{\text{p,stable}}^{\text{torso}}$ and $\dot{\theta}_{\text{r,stable}}^{\text{torso}}$ are the threshold of stable pitching and rolling angular velocity of the torso and k_p is the control gain.

4.4.2. Tilt over controller. The tilt over controller prevents KHR-2 from falling down in the lateral direction. If the humanoid becomes tilted due to unevenness of the ground on which it walks or due to the actions of external forces and obstacles, the robot may become unstable, or even fall down within few footsteps. There are two types of tilt over — outside tilt over and inside tilt over (Fig. 19). In general, inside tilt over is associated with much more risk than outside tilt over because next foot hits the ground strongly after the inside tilt over. The inside tilt over affects the next few footsteps, whereas outside tilt does not. As for the principles, during a short time τ from the start of the single-support phase (Fig. 8), the torso rolling angle is

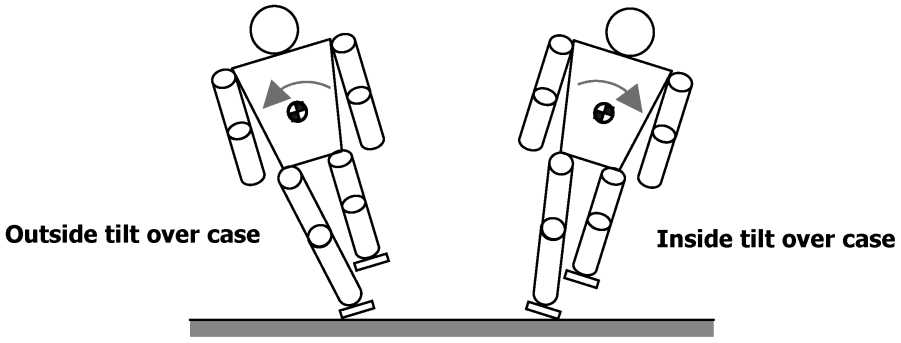

Figure 19. Two types of tilt over.

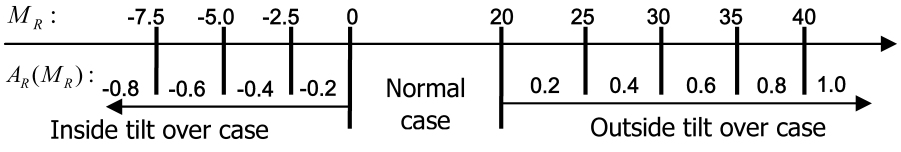

Figure 20. Map of the tilt over control.

integrated over time and then the tilt over case is judged by comparing that integral sum with the threshold derived previously from normal walking. If the integral sum exceeds the threshold values, the rolling angle of the ankle joint of the supported leg is immediately modified by adding a sinusoidal compensation according to the map (Fig. 20). The tilt over control law for right the foot is as follows:

$$\text{if } \int_{\text{Stage1,s}}^{\text{Stage1},\tau} \theta_{\text{r}}^{\text{torso}}\,\mathrm{d}t > V_{\text{Tilt over,out}} \text{ (outside tilt over) or}$$

$$\int_{\text{Stage1,s}}^{\text{Stage1},\tau} \theta_{\text{r}}^{\text{torso}}\,\mathrm{d}t < V_{\text{Tilt over,in}} \text{ (inside tilt over)},$$

then

$$\theta_{\text{m,r}}^{\text{R-ankle}}(t) = \theta_{\text{r}}^{\text{R-ankle}}(t) + A_{\text{R}}(M_{\text{R}}) \sin\left(2\pi \frac{t_{\text{c}}}{\tau'}\right) \text{ (deg) } \left(0 \leqslant t_{\text{c}} \leqslant \frac{\tau'}{2}\right), \qquad (15)$$

where $M_{\text{R}} = \int_{\text{Stage1,s}}^{\text{Stage1},\tau} \theta_{\text{r}}^{\text{torso}}\,\mathrm{d}t$ (deg), $V_{\text{Tilt over,out}} = 20$, $V_{\text{Tilt over,in}} = 0$, $V_{\text{Tilt over, out}}$ and $V_{\text{Tilt over,in}}$ are the threshold values of the outside and the inside tilt over, respectively, τ' is the duration of tilt over control, $\theta_{\text{r}}^{\text{torso}}$ is the rolling angle of the torso, A_{R} is the amplitude of the sinusoidal compensation and $\theta_{\text{r}}^{\text{R-ankle}}$ is the prescribed rolling angle of the ankle.

5. DYNAMIC WALKING EXPERIMENTS ON UNEVEN TERRAIN

We have carried out experimental tests and verified the capability of the dynamic walking algorithm of KHR-2. In our previous research [17], we studied the dynamic walking capability on flat, non-inclined surfaces and our previous humanoid robot could perform stable walking even when the parameters of walking pattern remained constant. In this work, we considered the inclinations and unevenness of real ground as well as its physical condition, such as slipperiness. Considering these issues, we improved the sole design (Fig. 21). First, the four points-supported sole was designed for the complete contact. Second, multi-layered rubbers were attached to absorb the high-frequency structural vibration caused by the shock during

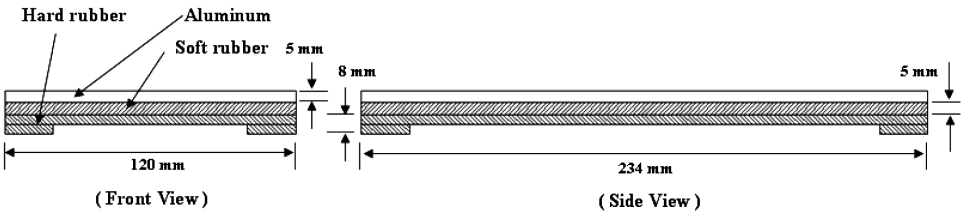

Figure 21. Sole design.

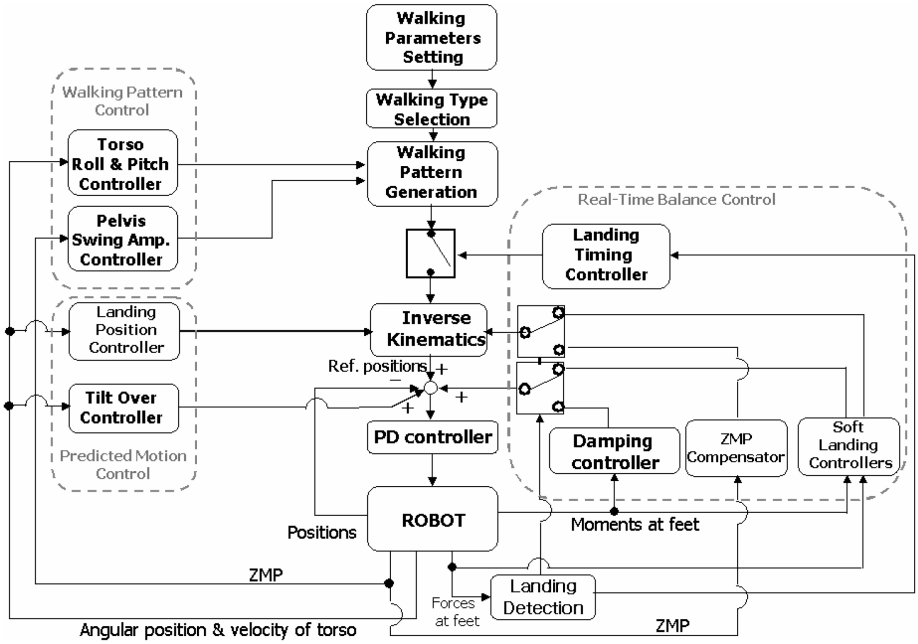

Figure 22. Schematic of the walking control algorithm.

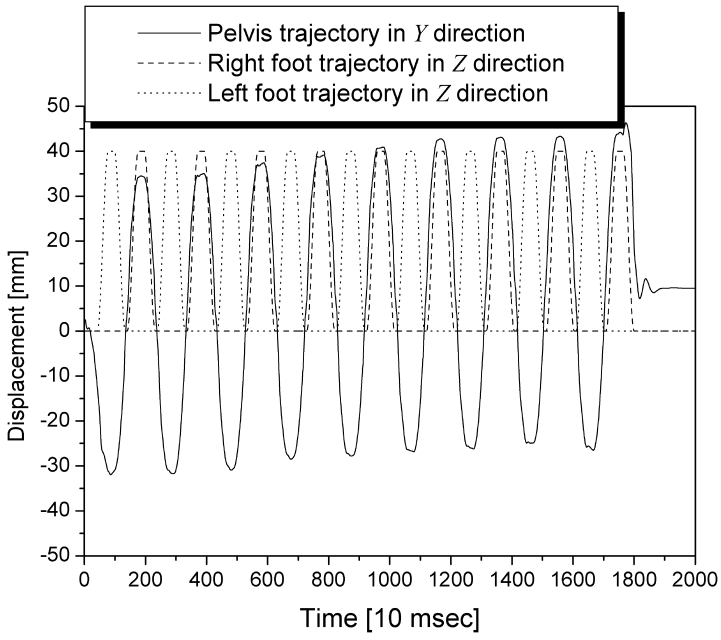

Figure 23. Forward walking pattern with a stride of 50 cm.

the landing. The reduction of high-frequency structural vibration is very important because it causes noise to the force/torque sensors. The rubber also provides resistance against slip.

The schematic of the dynamic walking algorithm is represented in Fig. 22. By using the algorithm, we tested dynamic biped walking of KHR-2 on a room floor which has an inclination of about $\pm 3^\circ$. Figure 23 shows the forward walking pattern that applied to KHR-2 during biped walking. It can be easily known that the pelvis center and its amplitude are changed gradually by the torso roll/pitch controller and the pelvis swing amplitude controller. Control inputs of those controllers are shown in detail in Fig. 24. Since the movements of KHR-2 is tilted forward (positive pitching angle) and right sideward (positive rolling angle), the pelvis center moves to backward and left sideward. Figure 25 represents control inputs of the damping controller and the landing orientation controller of the real-time balance control scheme. Figure 26 shows control inputs of the landing position controller and the tilt over controller of the predicted motion control. In the case of the tilt over control, it is observed that a more positive angle is added to the left rolling angle of the ankle because the robot was tilted right-sideward early. Finally, Figs 27 and 28 represent the attitude of the torso and the desired/actual ZMP during biped walking. In Fig. 27, the rolling and pitching angles of the torso are oscillated with amplitudes of about 1 and 1.5°, respectively. Initially those are tilted toward the positive region, but converged to near zero. In Fig. 28, the ZMP follows the desired value well within stable boundaries, so it can be known that dynamic biped walking was achieved successfully with good walking stability. Therefore, the effectiveness

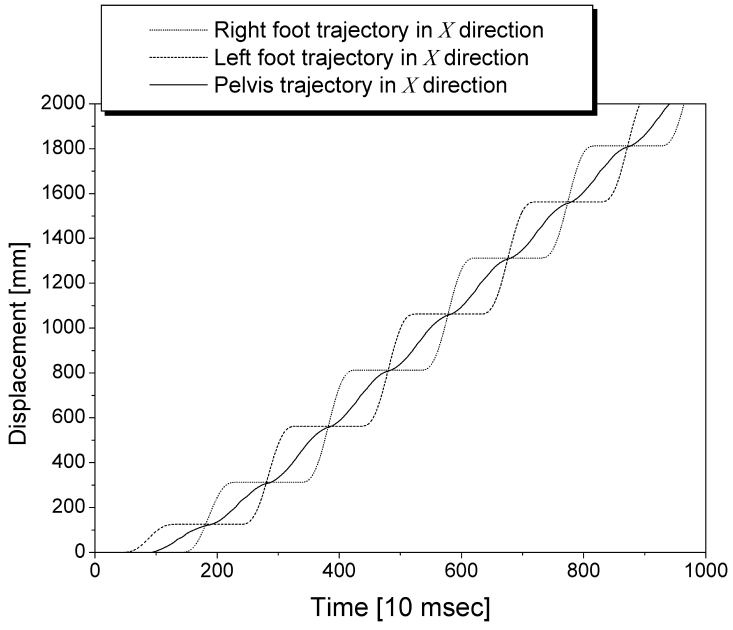

Figure 23. (Continued).

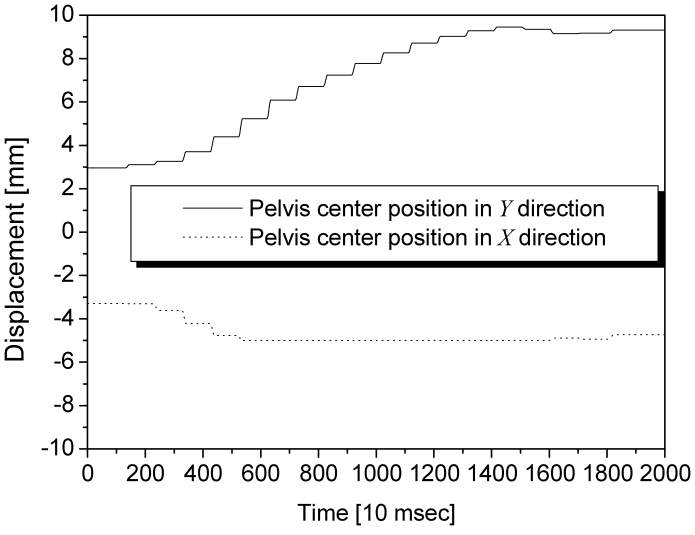

(a)

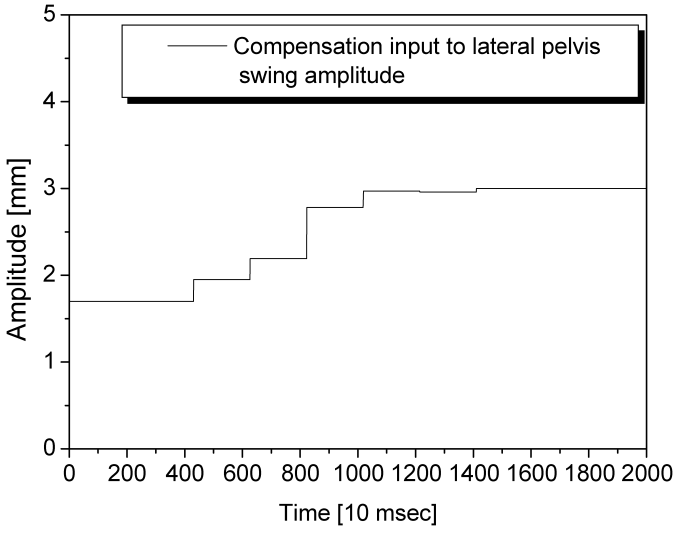

(b)

Figure 24. Walking pattern control. (a) Torso pitch/roll control. (b) Pelvis swing amplitude control.

of the dynamic walking control algorithm was proved experimentally. Figure 29 shows photographs of forward walking.

6. CONCLUSIONS

We have proposed a novel dynamic walking control algorithm for biped humanoid robots based on sensory devices such as force/torque sensors and inertial sensors.

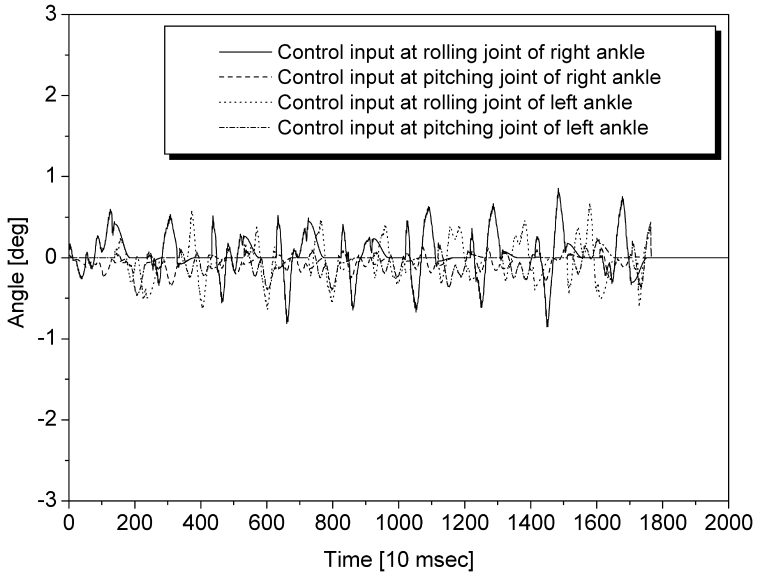

(a)

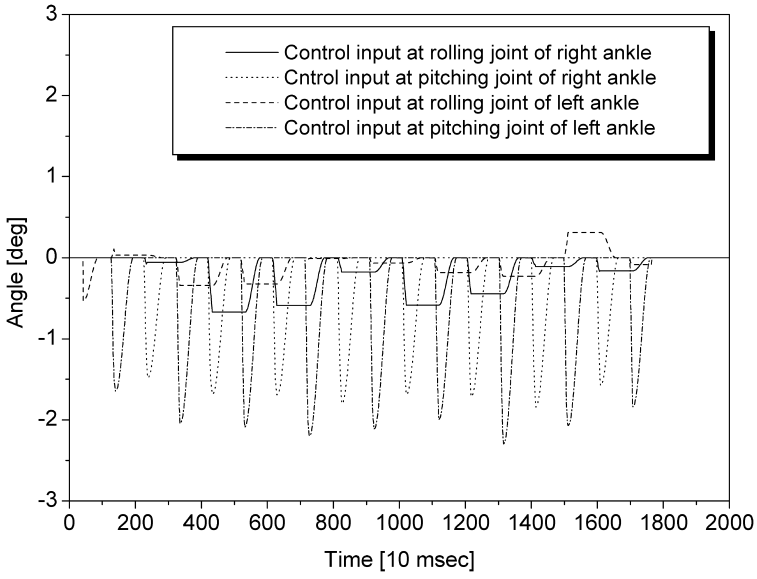

(b)

Figure 25. Real-time control inputs of (a) damping and (b) landing orientation controllers.

In this research, the biped humanoid robot platform KHR-2 was developed by designing all of the mechanical structures and hardware devices, including the motor controllers and the sensory devices, according to our design philosophy. The distributed control system architecture was integrated for KHR-2 so that it can be

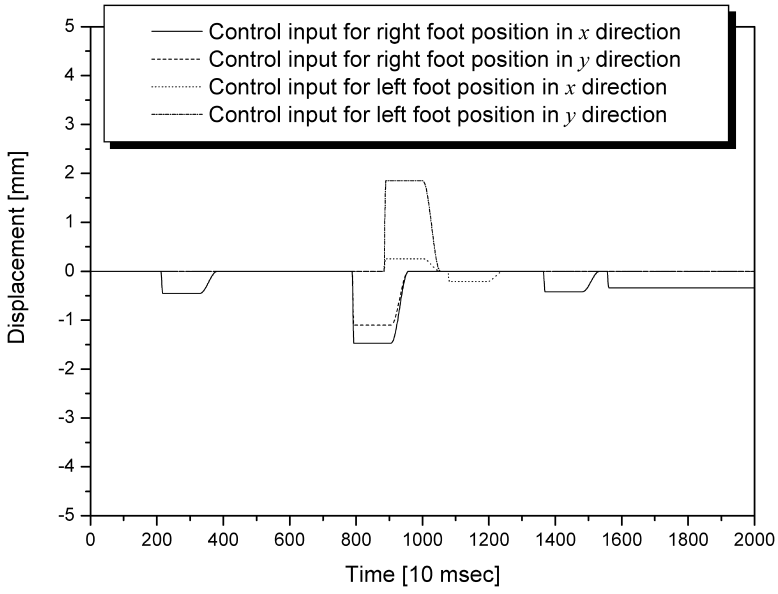

(a)

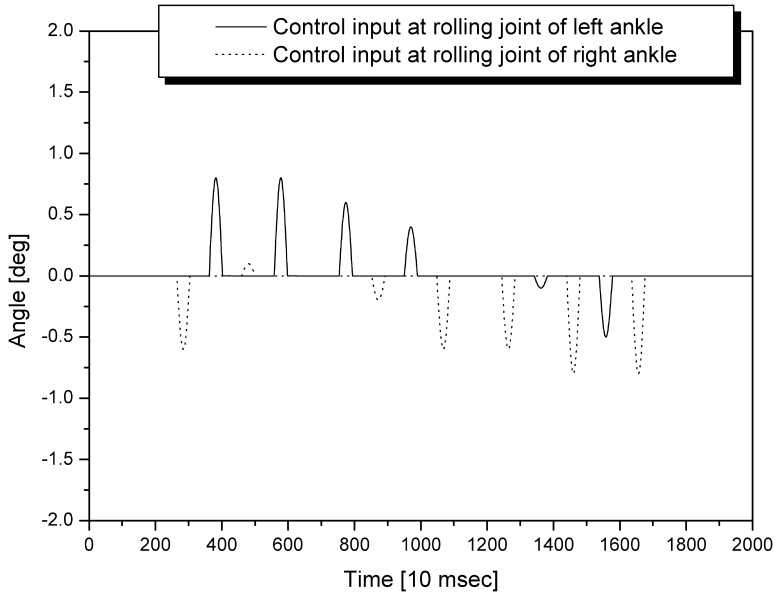

(b)

Figure 26. The predicted motion control. (a) Landing position control. (b) Tilt over control.

controlled with good efficiency and performance. As for the walking control, the motion control process was established first, and then the appropriate walking-ready pose was determined by considering the singularity problem of inverse

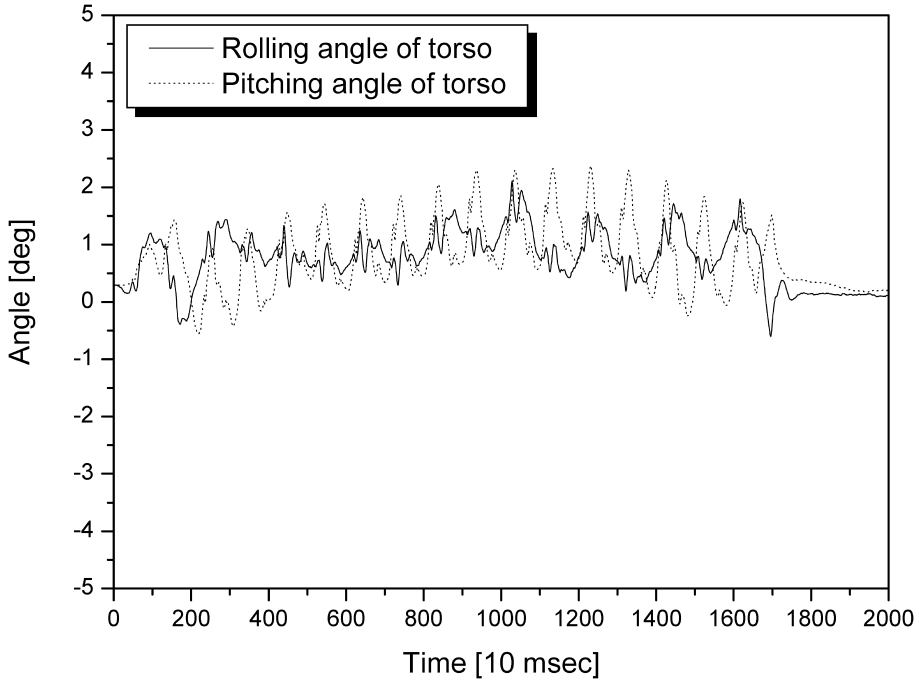

Figure 27. Attitude of the torso during forward walking.

kinematics, walking stability and the natural frequency of the inverted pendulum model. Second, the essential factors for walking pattern generation were defined and quantified by observing human movements and walking experiments of KHR-2. Third, the standard walking pattern of forward walking were designed and the walking stages were defined by dividing the walking pattern into five distinct stages. Fourth, three kinds of control schemes were established in order to design the online controllers for stable biped walking. These online controllers were designed according to the objectives of control schemes and planned in the walking stages. Finally, the walking control algorithm was integrated to KHR-2 and the sole design was upgraded to cope with the uneven ground conditions. The effectiveness of the proposed walking control strategy was verified by successful biped walking experiments.

Acknowledgements

This research was mainly supported by KAIST (Korea Advanced Institute of Science, and Technology) and partly supported by HWRS (Human Welfare Robotic System) and the BK-21 (Brain Korea-21) project.

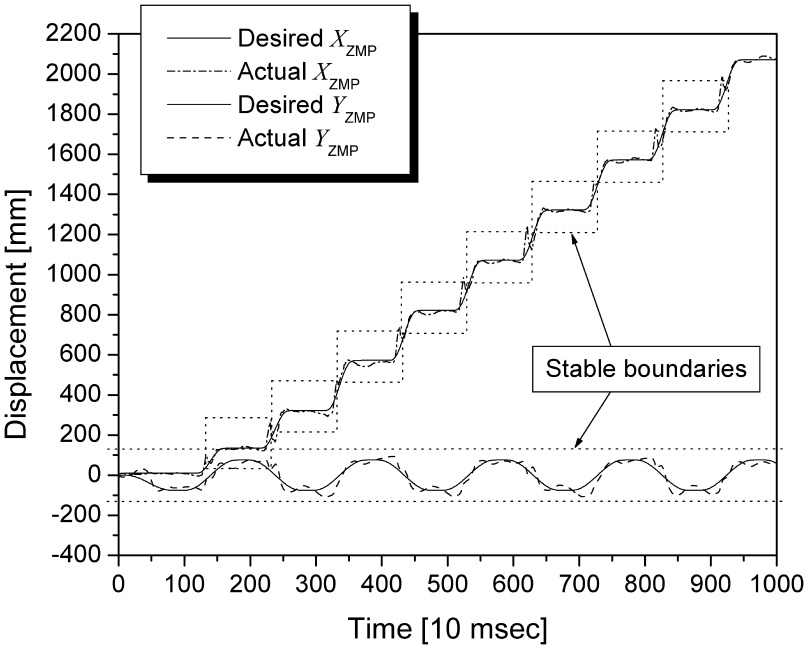

(a)

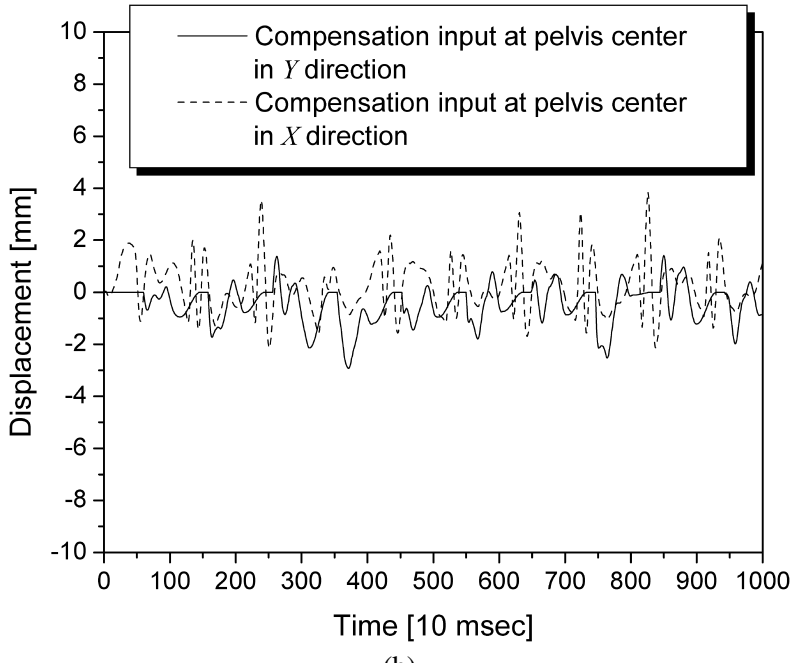

(b)

Figure 28. ZMP compensation.

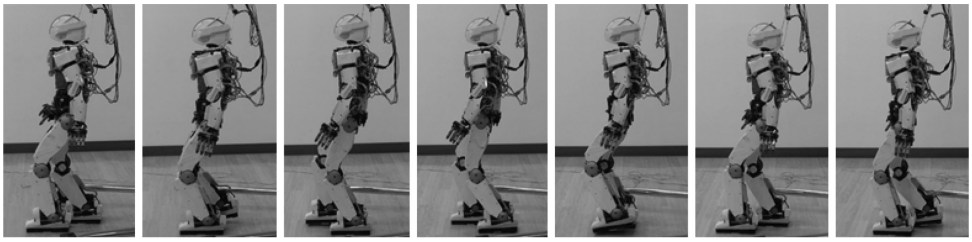

Figure 29. Photographs of the walking experiment.

REFERENCES

1. K. Hirai, Current and future perspective of Honda humanoid robot, in: *Proc. IEEE/RSJ Int. Conf. on Intelligent Robots and Systems*, Grenoble, pp. 500–508 (1997).
2. K. Hirai, M. Hirose, Y. Haikawa and T. Takenaka, The development of Honda humanoid robot, in: *Proc. IEEE Int. Conf. on Robotics and Automations*, Leuven, pp. 1321–1326 (1998).
3. Y. Sakagami, R. Watanabe, C. Aoyama, S. Matsunaga, N. Higaki and K. Fujimura, The intelligent ASIMO: system overview and integration, in: *Proc. IEEE/RSJ Int. Conf. on Intelligent Robots and Systems*, Lausanne, pp. 2478–2483 (2002).
4. J. Yamaguchi, A. Takanishi and I. Kato, Development of a biped walking robot compensating for three-axis moment by trunk motion, in: *Proc. IEEE/RSJ Int. Conf. on Intelligent Robots and Systems*, Yokohama, pp. 561–566 (1993).
5. H. Lim, Y. Kaneshima and A.Takanishi, Online walking pattern generation for biped humanoid robot with trunk, in: *Proc. IEEE Int. Conf. on Robotics and Automation*, Washington, DC, pp. 3111–3116 (2002).
6. K. Nishiwaki, T. Sugihara, S. Kagami, F. Kanehiro, M. Inaba and H. Inoue, Design and development of research platform for perception–action integration in humanoid robot: H6, in: *Proc. IEEE/RJS Int. Conf. on Intelligent Robots and Systems*, Takamatsu, pp. 1559–1564 (2000).
7. S. Kagami, K. Nishiwaki, J. J. Kuffner, Jr., Y. Kuniyoshi, M. Inaba and H. Inoue, Online 3D vision, motion planning and biped locomotion control coupling system of humanoid robot: H7, in: *Proc. IEEE/RSJ Int. Conf. on Intelligent Robots and Systems*, Lausanne, pp. 2557–2562 (2002).
8. K. Kaneko, F. Kanehiro, S. Kajita, K. Yokoyama, K. Akachi, T. Kawasaki, S. Ota and T. Isozumi, Design of prototype humanoid robotics platform for HRP, in: *Proc. IEEE Int. Conf. on Inteligent Robots and Systems*, Lausanne, pp. 2431–2436 (2002).
9. S. Kajita, F. Kanehiro, K. Kaneko, K. Fujiwara, K. Harada, K. Yokoi and H. Hirukawa, Biped walking pattern generation by using preview control of zero-moment point, in: *Proc. IEEE Int. Conf. on Robotics and Automation*, Taipei, pp. 1620–1626 (2003).
10. M. Gienger, K. Loffler and F. Pfeiffer, Towards the design of biped jogging robot, in: *Proc. IEEE Int. Conf. on Robotics and Automation*, Seoul, pp. 4140–4145 (2001).
11. V. T. Inman, H. J. Ralston and F. Todd, *Human Walking*. Williams & Wilkins, London (1981).
12. K. Mitobe, G. Capi and Y. Nasu, A new method for walking robots based on angular momentum, *Mechatronics* **14**, 163–174 (2004).
13. A. Goswami and V. Kallem, Rate of change of angular momentum and balance maintenance of biped robots, in: *Proc. IEEE Int. Conf. on Robotics and Automation*, New Orleans, LA, pp. 3785–3790 (2004).
14. M. Popovic, A. Hofmann and H. Herr, Angular momentum regulation during human walking: biomechanics and control, in: *Proc. IEEE Int. Conf. on Robotics and Automation*, New Orleans, LA, pp. 2405–2411 (2004).

15. M. Vukobratovic, B. Borovac, D. Surla and D. Stokic, *Biped Locomotion*. Springer-Verlag, Berlin (1990).
16. A. Bruderlin and T. W. Calvert, Goal-directed, dynamic animation of human walking, *Comp. Graphics (Proc. Siggraph)* **23**, 233–242 (1989).
17. J. H. Kim and J. H. Oh, Realization of dynamic walking for the humanoid robot platform KHR-1, *Advanced Robotics* **18**, 749–768 (2004).
18. J. Y. Kim, I. W. Park, J. Lee, M. S. Kim, B. K. Cho and J. H. Oh, System design and dynamic walking of humanoid robot KHR-2, in: *Proc. IEEE Int. Conf. on Robotics and Automation*, Barcelona, pp. 1443–1448 (2005).

ABOUT THE AUTHORS

Jung-Yup Kim was born in Seoul, South Korea, in 1976. He received the BS and MS degrees in Mechanical Engineering from Inha University, Incheon, South Korea, in 1999 and 2001, respectively. He is currently a Graduate Student of the PhD course in the Department of Mechanical Engineering, KAIST. His research interests include design and control of biped humanoid robots, visual processing, development of sensory devices using micro processor, and tele-operated system. He is a member of the KSME and ICASE.

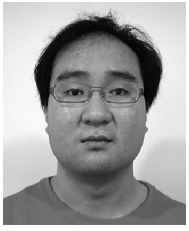

Ill-Woo Park was born in Seoul, South Korea, in 1977. He received the BS and MS degrees in Mechanical Engineering from KAIST, in 2000 and 2002, respectively. He is currently a Graduate Student of PhD course in the Department of Mechanical Engineering, KAIST. His research interests include humanoid robot design and biped walking control.

Jun-Ho Oh was born in Seoul, South Korea, in 1954. He received the BS and MS degrees in Mechanical Engineering from Yonsei University, Seoul, South Korea and the PhD degree in Mechanical Engineering from the University of California, Berkeley, USA, in 1977, 1979 and 1985, respectively. He was a Researcher with Korea Atomic Energy Research Institute from 1979 to 1981. Since 1985, he has been with the Department of Mechanical Engineering, KAIST, where he is currently a Professor. He was a Visiting Research Scientist in University of Texas, Austin, TX, USA, from 1996 to 1997. His research interests include humanoid robots, adaptive control, intelligent control, non-linear control, biomechanics, sensors, actuators and application of micro processors. He is a member of the IEEE, KSME, KSPE and ICASE.